

Research

Structural design and adaptive tracking control of automatic welding robot for liquefied natural gas containment system

Yunze Chu^{1,2} · Kejing Ma² · Liang Zhao³ · Jun Xu³ · Wenxin Zhou² · Xu Wang² · Haiping Guo² · Yansong Zhang¹

Received: 30 September 2023 / Accepted: 28 February 2024

Published online: 08 March 2024

© The Author(s) 2024 [OPEN](#)

Abstract

Liquefied natural gas (LNG) is commonly transported by LNG carriers and stored in cargo containment systems. The primary barrier of the MARK III cargo containment system is welded to a closed space with corrugated stainless steel plates. To meet the requirements of excellent sealing and thermal insulation for cargo containment, the welding process of the corrugated plate need to be strictly controlled, which poses a challenge to the development of related welding equipment. In this paper, we present a new five-axis automatic welding robot system used for plasma arc welding on corrugated surfaces. The moment transfer scheme of the dual linkage mechanism makes the rotary movement of the robot more accurate and stable which gives the system with simpler control algorithm and better overall force characteristics. To ensure tracking accuracy, a novel sensing method based on a LASER sensor, two contact sensors, and an angle sensor is proposed to implement multiple functions such as tracking the welding arc length, identifying corrugation shapes, and detecting welding gun posture. Based on the devised tracking sensor system and welding robot, a servo-control system with a surface-tracking welding control algorithm is established. The experimental results show that the robot system's welding speed is about 7 times that of hand welding and the welding qualification rate was 99%, significantly improving welding efficiency and quality as a critical equipment technology in the process of corrugated plate welding.

Article Highlights

- (1) A new five-axis automatic welding robot system based on a surface tracking control algorithm is designed for plasma arc welding on corrugated surfaces, which can realize flat, horizontal, vertical, and overhead automatic welding in LNG liquid cargo containment.
- (2) A novel tracking sensor system based on a laser sensor, two contact sensors, and an angle sensor is proposed to implement multiple functions such as tracking the welding arc length, identifying corrugation shapes, and detecting welding gun posture.
- (3) The sensing system can cooperate with the robot servo-control system to complete welding seam tracking, adjustment and control of welding gun spatial posture. The experimental results show that the robot system's welding speed is about 7 times that of hand welding and the welding qualification rate was 99%, which reflects that the robot servo-control system can complete the welding of corrugated structures in the cargo containment with high quality and high efficiency welding.

✉ Kejing Ma, Sarah_mkj@163.com | ¹Shanghai Key Laboratory of Digital Manufacture for Thin-Walled Structures, Shanghai Jiao Tong University, Shanghai 200240, People's Republic of China. ²Shanghai Shipbuilding Technology Research Institute, Shanghai 200240, People's Republic of China. ³Hudong-Zhonghua Shipbuilding (Group) Co., Ltd., Shanghai 200240, People's Republic of China.



Keywords Welding robot · Structural design · Liquefied natural gas carrier · Surface tracking control

1 Introduction

With the growing demand for clean environmental energy, the usage of natural gas has been increasing every year, leading to an increase in liquefied natural gas (LNG) ship transportation [1, 2]. The MARKIII cargo containment system, which stores liquid LNG at a temperature of $-163\text{ }^{\circ}\text{C}$, is a crucial technology for LNG ships [3–7]. The primary barrier of the MARKIII cargo containment system, made of 304L corrugated stainless steel plates, is essential in withstanding swaying loads [8]. The whole cabin is formed by completely continuous and dense 1.2 mm thick stainless steel films with crisscrossing corrugations, in which the size of a single corrugated plate is $1\text{ m} \times 3\text{ m}$ [9]. The corrugated plate of the primary barrier is sealed by the lap of each part, and the lap is welded by plasma. The main technical difficulty of the MARKIII cargo containment system is the welding and inspection of the corrugated area. Ultrasonic and other non-destructive testing methods cannot detect the internal welding quality of the stainless steel film. Therefore, it is necessary to strictly control the welding process to achieve good welding results. The welding quality of the corrugated plate is crucial to the integrity of the main screen wall, which is key to the successful construction of the LNG ship containment system. Thus, it is essential to study the welding technology of corrugated plates in MARK III cargo containment systems. Because the shipyard welding task has the characteristics of non-standard, small batch, and large workpieces, robotic welding systems are seldom studied [10–12]. Manual welding is not only inefficient and low-quality but also a safety risk for workers [13, 14].

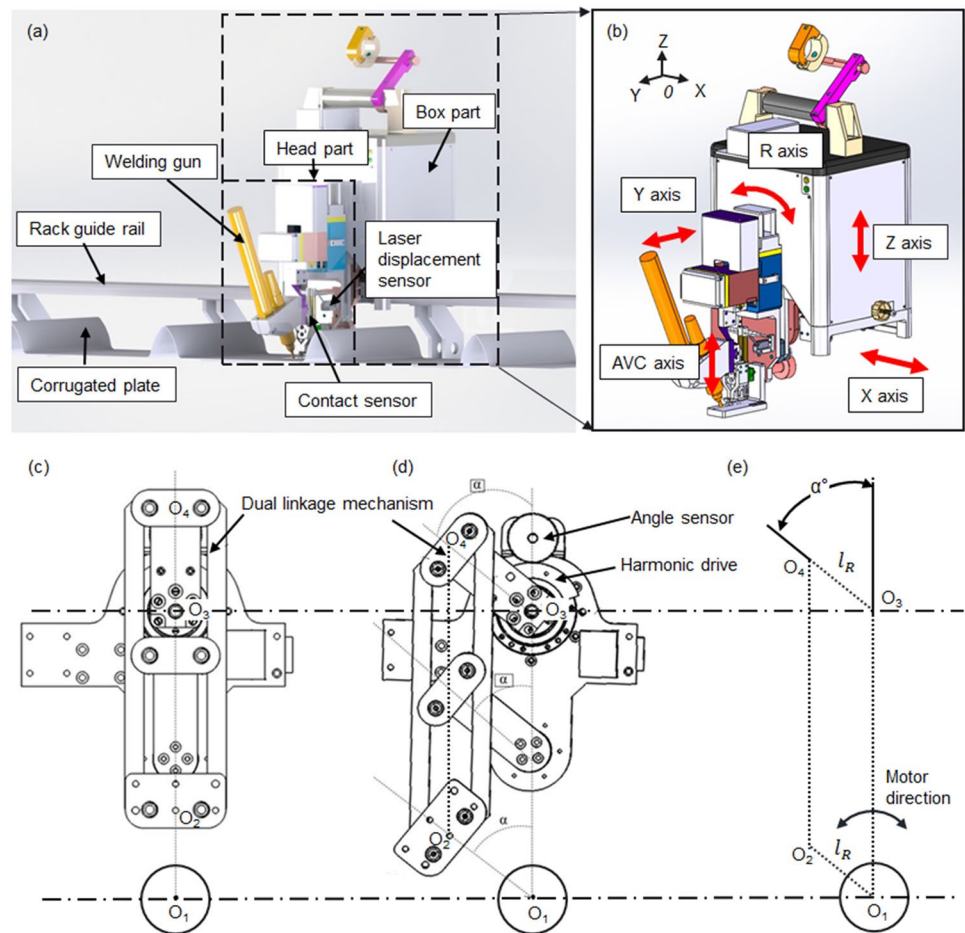
In recent years, several welding robots have been proposed to improve the automation level of ship welding [15–17]. A plasma welded spider robot automatic transfer system for membrane corrugated plates of LNG Carrier (LNGC) was proposed [18]. However, the spider robot has low stiffness, large weight, easy torsion of the robot body, and is unable to carry out high-position welding tests. A series–parallel-series hybrid mobile welding robot was proposed for membrane tank welding in LNG ships [19]. An autonomous mobile welding robot based on an embedded industrial computer was designed and developed for discontinuous weld seams in shipbuilding [20]. A small robot composed of a 6-axis modular controller, a 3P3R serial manipulator, and an auxiliary transport device is proposed for welding U-shaped trajectories in enclosed space [21]. A welding robot system based on visual servo control was designed to realize the automatic welding of box steel girders in all spatial positions [22]. The welding robot is composed of left and right wheels, vertical sliding blocks, horizontal sliding blocks, rotating joints, arc guns with rotating arc sensors, ultrasonic sensors, photoelectric position sensors, and universal wheels, capable of achieving rectangular fillet weld tracking in shipyards and steel structure workshops [23]. However, the existing robots are complex in structure and lack a welding quality index. Moreover, the welding speed and efficiency of some welding robots are not high. Therefore, it is necessary to develop automatic welding equipment for adapting various corrugated shapes, which should have a high welding qualification rate, high welding efficiency, and meet the welding of all spatial positions [24].

We designed a welding robot system based on a LASER sensor, contact sensors, and an angle sensor to meet high-quality requirements for welding corrugated structures in cabin conditions. The structure of the welding robot is designed with a dual linkage mechanism to form a virtual rotating shaft, enabling the welding gun to rotate around the welding gun's fire point. In the welding robot control system, a surface tracking control algorithm is used to realize real-time path planning. This equipment can be flexibly adjusted according to different radii of large and small corrugations in the welding process. Ultimately, the welding robot system can automatically track the corrugated plate welding, and realize the improvement of welding quality and efficiency.

2 Structural design of welding robot

The design objective of the five-axis welding robot is to enable the welding gun to move precisely along the corrugated welding seam path. Figure 1a illustrates the three-dimensional design model (SolidWorks) of the plasma welding robot. The welding robot is mainly composed of a rack guide rail, a supporting mechanism, and a machine body. The upper end of the supporting mechanism is affixed with the rack guide rail, on which the machine body is placed. The machine body's gear and the rack on the support work together to drive the machine body's motion along the X direction. The rack guide rail and the supporting mechanism not only play the role of limiting and guiding the machine body moving

Fig. 1 Schematic diagram of the welding robot **a** design model of the welding robot, **b** motion direction diagram of the welding robot, **c** the initial position of the rotating motor, **d** the motor rotation angle of α° , **e** schematic diagram of rotation



along the X direction but also act as load-bearing capacity to avoid damage to the corrugated plates. Nylon limit blocks are positioned at either end of the support to prevent the machine body from falling off.

The welding robot system utilizes a software programmable logic controller (PLC) to control five motor servo drivers that drive the robot's brushless DC electric motor. These motors are responsible for linear motion, rotation motion, and motion compensation. Table 1 provides the parameters of each motor. The machine body is divided into two parts: the box and the head, which contains the welding gun. The X, Z, and R axes motor are located in the box part, which is connected to a guide rail that can be tightened or separated by a buckle (Fig. 1b). The guide rail is positioned along the X direction. The X-axis motor is installed on the bottom and connected to the guide rail by a gear rack mechanism. This motor drives the entire robot to move along the guide rail using a gear drive. A vertical lead screw is provided in the box, and the Z-axis motor provides power to the synchronous belt wheel and synchronous belt to drive the lead screw. The slide rail slider acts as a fine guide to control the robot's Z-direction movement. This controls the vertical distance between the welding gun and the corrugated plate. The R-axis is responsible for the rotation and uses a harmonic drive reducer to achieve precise angle control. To transfer the R-axis's rotation center to the welding gun's fire point, a dual linkage mechanism is used, as shown in

Table 1 Motor parameters

Motor	Velocity	Maximum Rotational speed	Reduction ratio
X-axis traveling motor	0–6 mm/s	4000 RPM	415: 1
Z-axis traveling motor	3–6 mm/s	4000 RPM	66: 1
R-axis rotating motor	0– $\pi/6$ rad/s	4000 RPM	1120:1
Y-axis adjustment motor	0–5 mm/s	12,000 RPM	43: 1
AVC-axis adjustment motor	0–5 mm/s	12,000 RPM	43: 1

Fig. 1c–e. The design advantages of the dual linkage mechanism are mainly embodied in two aspects. (i) Transfer the R-axis rotation center to the welding gun fire point to complete the replication of motion. (ii) By controlling the rotation of the R-axis to control the rotation of the welding gun, the complexity of the control code of the robot system in the corrugated plate welding can be effectively reduced, and the welding reliability can be improved. This mechanism utilizes two T-plates and two vertical connecting plates to form two parallelogram structures. The R-axis's rotation center O_3 and the virtual rotation center O_1 are located on the rotation center line formed by connecting the ends of two T-plates. The rotation radius O_3O_4 of the R-axis is equal in length to the rotation radius O_1O_2 of the virtual rotation center O_1 . The tails of the two vertical connecting plates are connected to the head part, transferring torque to the welding torch on the head part and completing the duplication of motion. The virtual axis O_1O_2 rotates around the center of rotation O_1 to ensure that the welding gun always points to the center of the circle O_1 .

The X, Z, and R axes control the entire head part, including all sensors and a welding gun. The welding gun is fixed to the front of the head part and driven to the desired position and posture for welding through the robot's movement. The box part of the robot provides the X-direction displacement, Z-direction displacement, and the R-axis rotation for the welding gun. The welding robot head is equipped with motion mechanisms for the Y-axis and AVC axis. These mechanisms are used to fine-tune the position of the welding gun in the Y and welding gun directions during welding. The aim is to compensate for any discrepancy between the theoretical and actual displacement of the welding gun. The AVC axis is responsible for compensating for any displacement along the welding gun, therefore ensure that the welding gun is always perpendicular to the surface of the corrugated surface, while the Y axis is connected to the AVC axis motor. The Y axis compensates for the displacement of the welding gun in the Y direction, which is the horizontal direction of the weld seam. Additionally, the welding robot head features a range-ranging LASER sensor that detects changes on the plate surface to determine the type of corrugated plate. Two contact displacement sensors are positioned on the fixed bracket of the welding gun adjusting mechanism, one is installed 2 mm behind the other. Table 2 shows the specification of sensors and welding gun.

3 Welding robot sensing system

The sensor system comprises an angle sensor, two contact sensors, a LASER displacement sensor, and seven proximity switches. The angle sensor is connected to the R-axis for measuring the rotation angle of the welding gun (Fig. 1d). The contact sensors provide a resolution of 1 μm and are used for automatically tracking the welding gun position and welding arc length. Each contact sensor includes a contact sensor head (ruby probe) and tail amplifiers (tactile sensor body). To ensure tracking accuracy, two ruby sensor probes are used near the welding gun's end, and two tactile sensors are placed far away from the welding gun's end, preventing damage from welding sparks. The two contact sensors, namely Sensor No. 1 and Sensor No. 2, are located 2 mm apart in the x direction. Sensor No. 1 is positioned at the head of the welding gun in the x direction, while Sensor No. 2 is situated ahead of Sensor No. 1 in the x direction. By measuring the change in the height of the ruby head in contact with the corrugated plate, the system can detect corrugations and plane irregularities, which can then be used to determine tracking errors. The contact displacement sensors serve three specific functions. Firstly, they are used to detect the distance between the welding gun and the weld seam, and provide corresponding feedback when the plate undergoes local deformation. The PLC control motor drives the welding gun to adjust the z-direction distance between the welding gun and the weld seam, which effectively ensures the welding quality. Secondly, by comparing the height difference detected by two contact sensors, they can judge the starting point of the trajectory of the corrugation plate shape. Thirdly, the real-time trajectory of the welding gun is calculated by substituting the values of the contact sensors into the surface tracking control algorithm. Accurate determination of the welding gun's entry into the corrugation time is possible through the relative value measured by the contact sensor. Therefore, the PLC sends the position instruction to the welding gun to go over the corrugation trajectory, which in turn ensures welding quality stability. The contact sensor has a range of 10 mm. After calibration, we set the midpoint of the range as the initial. The 0 μm indicates that the welding gun has reached the initial position, and the reference value of the sensors during the welding process may change with manual intervention.

The distance between the contact sensor and the LASER sensor in the x direction is approximately 15 mm. The main functions of the LASER sensor are as follows: firstly, to determine the detection starting point of the contact sensor, and secondly, to determine the size of corrugated plates. The LASER displacement sensor detects changes in the plate surface

Table 2 Specification of sensors and welding gun

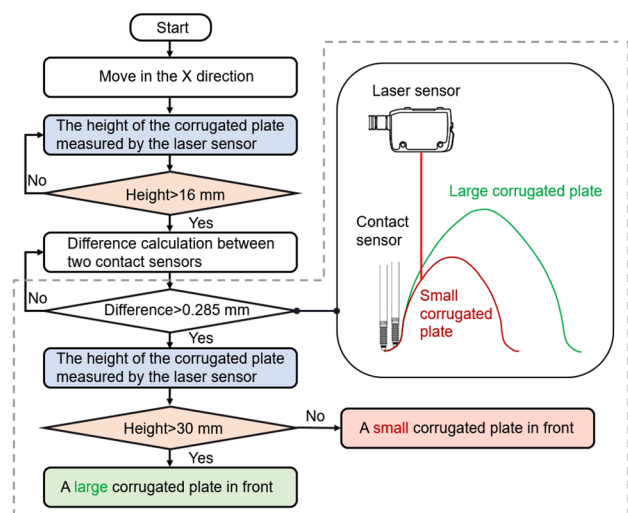
Element	Contact sensor	LASER sensor	Welding gun
Specification	PETER HIRT GmbH T502F	KEYENCE LR-X100	NSC 51KWH

to determine the type of corrugation and controls the light flicker through the signal transmission to notify the operator that the robot is entering the corrugation area for welding. Two LASER values, 16 mm and 30 mm, are used to determine the presence of corrugations. The flowchart in Fig. 2 illustrates the process of corrugation detection. During the welding process, when the LASER displacement value exceeds 16 mm, the contact sensor feedback signals to PLC. At this point, the difference between the two contact sensors in the z direction is denoted by Δ . When the No. 1 contact sensor is at the corrugation origin, according to the shape of the corrugation, the height of the No. 2 contact sensor at the position of 2 mm forward on the corrugation is about 0.285 mm. In order to prevent the 0.285 mm caused by welding jitter and other reasons, it is necessary to predict the appearance time of corrugation in advance by the LASER sensing value. When the contact sensor reaches the corrugation origin, the LASER sensor measures the height of the corrugation at the position 15 mm away from the corrugation origin. At this time, the height of the large corrugation is about 32 mm, and the height of the small corrugation is about 28 mm. The average height of the large corrugation and small corrugation measured by the LASER sensor is 30 mm. Take 16 mm, half of the height of the large corrugation, as a pre-judgment, the contact sensor is about to enter the corrugation section and start the measurement. The corrugation origin is detected when the difference between the two contact sensors in the z direction is $\Delta + 0.285$ mm. At this point, the second set value of the LASER displacement sensor is read to determine the corrugation size. If the return value of the LASER displacement sensor is greater than 30 mm, the robot judges a large corrugated plate in front; otherwise, it judges a small corrugated plate in front. A proximity switch is provided on the welding robot, and a detected block is placed at one end of the bracket to signal the PLC to stop the motor when the robot reaches the end of the bracket. The proximity switch and nylon limit block work together to prevent the welding robot from falling off when it reaches the limit.

4 Control system

The control system for the corrugated plate welding process is mainly integrated into a control cabinet. The control cabinet serves as the main interface for managing the system's functionality, such as setting and modifying welding parameters for each arc of the corrugated plate, controlling input/output for the welding robot, and transmitting or receiving data with the welding robot. In addition, the control cabinet facilitates welding speed conversion and automatic arc length tracking. The cabinet consists of a touch screen, ethernet switch, communication module, wireless remote receiver, digital and analog input/output (I/O) module, and an industrial computer (IPC). The communication module is responsible for collecting data from both digital and analog I/O modules, and transmitting it to an industrial computer. The digital and analog I/O modules receive signals from various sensors. With a cycle time of 1 ms, the PLC acquires and processes sensor data in real-time, thereby minimizing errors in contact sensor and LASER sensor values. This ensures that any errors are immediately detected and addressed. The CODESYS (V3.5SP17) soft PLC in IPC is used to control a servo motor that drives a welding robot. The PLC is responsible for controlling the motor to adjust the distance between the welding gun and the weld seam, which helps to ensure high-quality welding. The software PLC includes several different modules, such as Control RTE (real-time control), SoftMotion (single-axis and master-slave axis motion

Fig. 2 The flowchart of corrugation detection

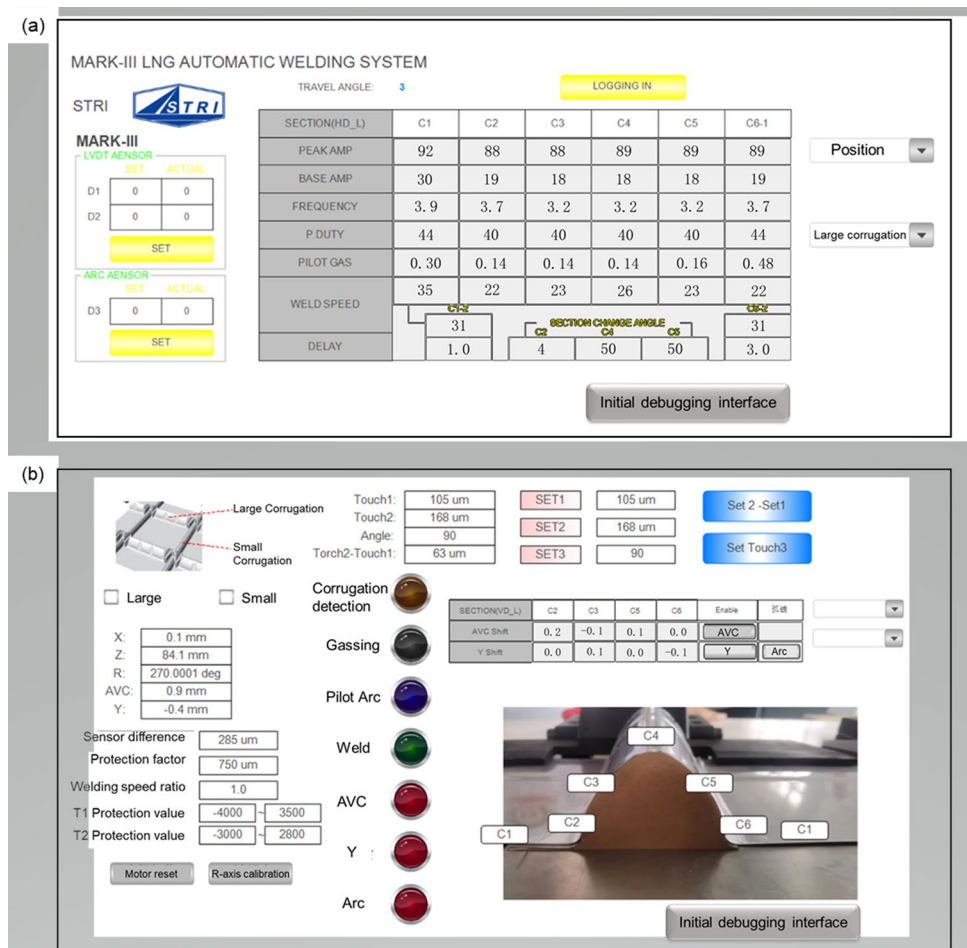


control, electronic CAM), CNC + Robotics (interpolation numerical control and robot motion control), TargetVisu (local visualization), and other related modules.

4.1 Control interface

The industrial computer contains a welding process parameter database, which enables the PLC to send a group of process parameters to the welding power in order to change parameters at any time via serial communication. These welding process parameters include travel angle, peak current, base current, pulse frequency, duty ratio, pilot gas velocity, and welding speed. The industrial computer can control the operation of arc starting, clear the welding gun, and emergency stop. In addition, the robot is also equipped with a touch screen which is convenient for operators to modify welding parameters and monitor equipment status. The touch screen of the welding system is equipped with two switchable interfaces. The first interface, depicted in Fig. 3a, is used to display and adjust the process parameters that are sent to the welding power source. The second interface, shown in Fig. 3b, is dedicated to setting and displaying the welding robot-related parameters. To ensure accurate measurements during the welding process, it is necessary to set the initial position of the contact sensor and the return value of the angle sensor measured by the calibration block. The difference between the two contact sensors ($\Delta + 285 \mu\text{m}$) is used as the starting point for the corrugation judgment. If the value of contact sensor 2 reaches $750 \mu\text{m}$ before triggering the set value of $\Delta + 285 \mu\text{m}$, the incoming wave protection value of $750 \mu\text{m}$ is activated to start the emergency stop. Furthermore, the touch screen displays the real-time motor positions of the five axes, which are fed back by Hall sensors inside the servo motor. The automatic compensation values of the AVC axis and Y axis in different corrugation sections are also shown. The operating status of the welding robot is displayed through indicator lights.

Fig. 3 Switchable interfaces **a** touch screen welding process parameter adjustment interface, **b** main interface sensor data and main switch monitoring



4.2 Motion trajectory control

The thin-film LNG cargo containment system's primary layer screen wall consists of a 1.2 mm thick 304 stainless steel plate with corrugated squares in vertical and horizontal directions. These squares have a length of 340 mm and are made up of multiple vertical large and small corrugations intersecting with one another. The corrugated plate profile model is composed of lines and arcs. Figure 4 shows that the welding equipment uses the output signal of the contact sensor No. 1 to determine the actual position of the welding gun on the corrugated plate surface. The servo motor adopts the PID control algorithm, among which cyclic synchronous position mode (CSP) is used for position control. The industrial computer transmits the position on a theoretical waveform to the DC motor every 1 ms, controlling the X, Z, and R axes' motion.

Figure 5 illustrates the real-time compensation closed-loop control system. During welding, the difference between the real-time contact sensor No.1 height and the initial position height is calculated. The welding trajectory comprises both flat and corrugated sections. In the flat section, the welding robot mainly controls the movement of the X-axis. The PLC controls the Z-axis motor to compensate welding height difference. The Z-axis motor's target position is calculated as the sum of its real-time position and the sensor height difference. During corrugation section welding, the LASER sensor and contact sensor determine the corrugation's initial position and size. The contact sensor No. 1 tracks the welding arc length in real time and applies the linear change value between its real-time height and the set position to the AVC axis of the robot head to achieve accurate tracking of the welding position. The target position of the AVC-axis motor is calculated as the sum of its real-time position and the sensor height difference. The AVC-axis compensates for displacement in the direction of the welding gun. The return value of contact sensor No. 1 (t_1) should be close to 0 μm , otherwise the AVC axis automatically compensates for the difference between the actual value of contact sensor No. 1 and 0. The AVC axis boasts an impressive tracking accuracy of ± 0.1 mm, which guarantees precise and consistent welding performance.

4.3 Surface tracking control

To realize the adaptive welding of arbitrary surfaces, the surface tracking welding control algorithm is proposed. Using the real-time values of the contact sensors and the 3-axis synchronized motion control system, the moving path of the welding gun in the (x, z) plane is calculated. The welding gun and contact sensor No. 1 are located in the same x and z position and have the same motion trajectory. Therefore, the forward trajectory of contact sensor No. 1 is the forward direction of the welding gun. As shown in Fig. 6, T1 and T2 represent contact sensor No.1 and contact sensor No.2, respectively. Along the welding direction, the welding gun goes from the T1 position to the T2 position, and the actual distance traveled is L. The distance L is projected into the x and z directions to calculate change values in the two directions. Since the welding gun must always be perpendicular to the corrugated surface, the welding gun will have to rotate the α angle perpendicular to the corrugated surface once it reaches T2. The position analysis of the welding gun for surface tracking welding indicated that the moving path of the welding gun can be calculated in real time through the sensors and the angle of the welding gun. The end trajectory of the welding gun in the (x, z) plane could be expressed by Eq. 1:

Fig. 4 Block diagram of welding robot control system

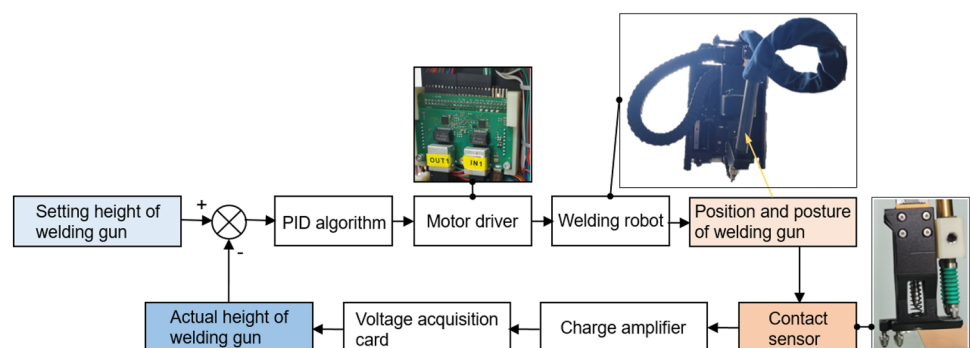


Fig. 5 Real-time compensation closed-loop control system

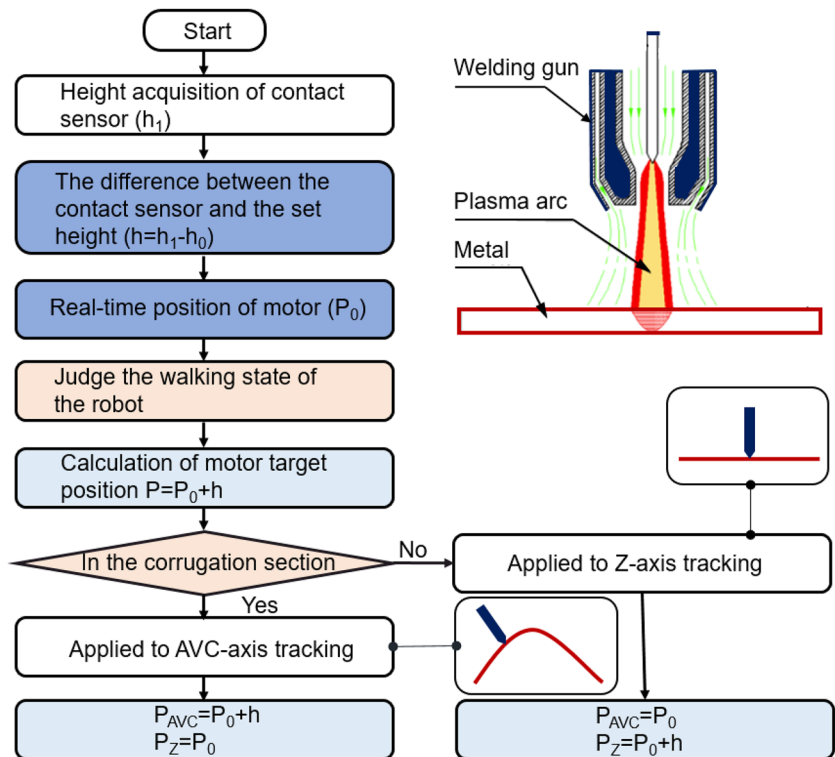
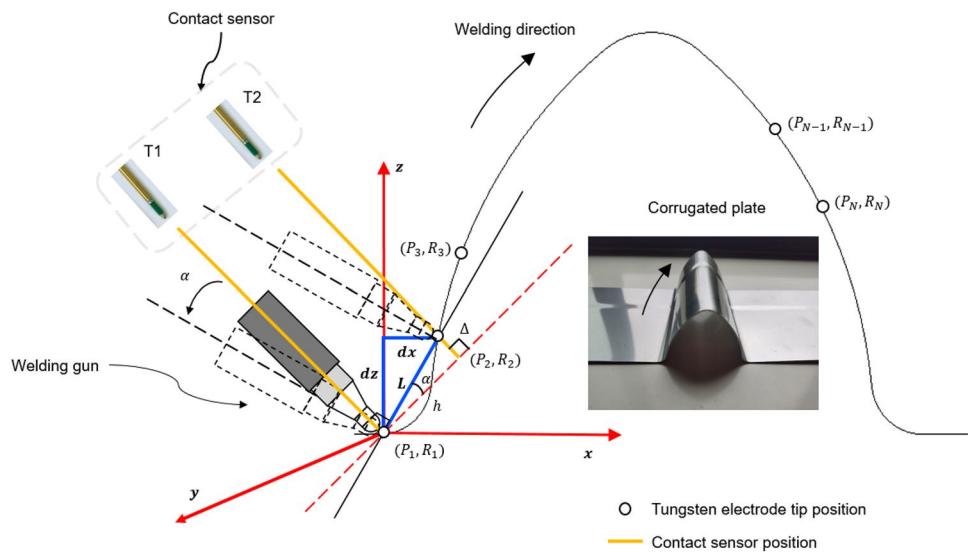


Fig. 6 Schematic diagram of calculation method of welding gun moving track along corrugated plate



$$\begin{cases} dx = L * \sin\theta \\ dz = L * \cos\theta \\ \alpha = \arctan(\Delta/h) \end{cases} \quad (1)$$

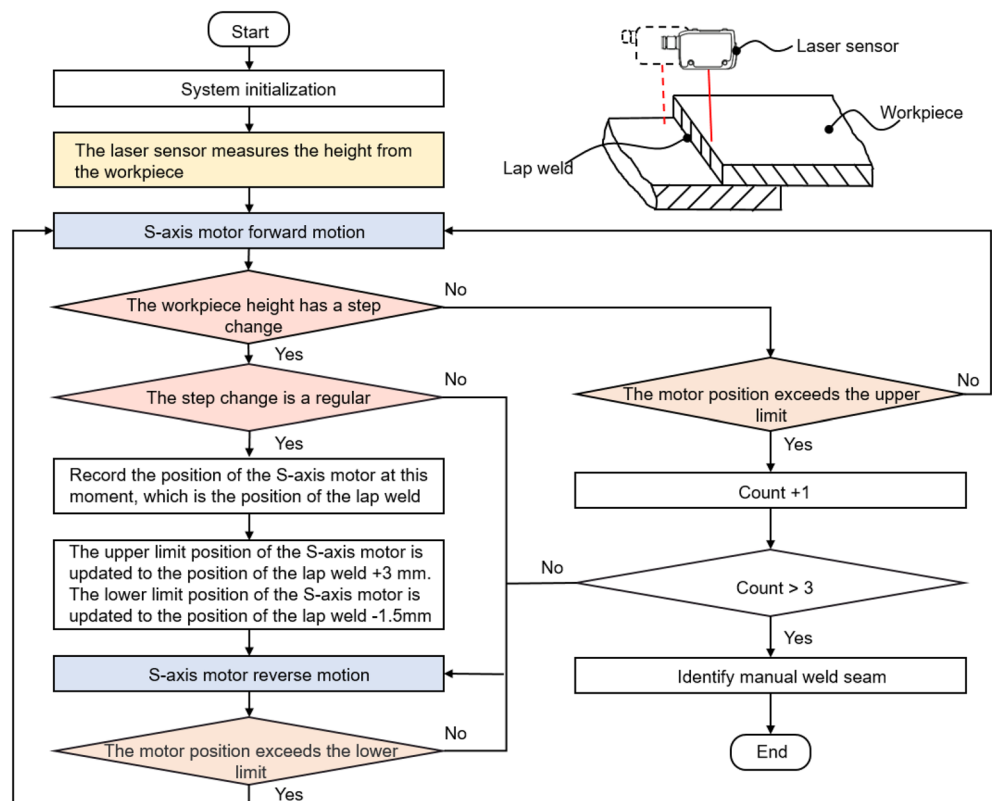
where $L = \sqrt{\Delta^2 + h^2}$ is the distance between the end of contact sensor No. 1 and contact sensor No. 2. Δ is the difference between the two contact sensors in the direction of the welding gun. h is the distance between parallel lines of contact sensor No. 1 and contact sensor No. 2. $\theta = \frac{\pi}{2} - \alpha - \frac{R}{180} * \pi$ is the angle between the connecting line of the contact sensors and the Z-axis. R is the angle of the welding gun. dx is the calculated target displacement of the welding gun in the X-direction. dz is the calculated target displacement of the welding gun in the Z-direction. α is the calculated R-axis target angle of the welding gun. The tracking error is the difference (t_d) between the actual value of contact sensor No. 1 and

the set value ($0 \mu\text{m}$), which is compensated by the Z-axis. The compensation value of the Z-axis can be expressed as $t_d * \cos\left(\frac{R}{180} * \pi\right)$.

The displacement of the welding gun in the (x, z) plane is controlled by X and Z axes motors, while the other direction displacement in the three-dimensional space is controlled by the Y-axis motor. In order to realize Y-direction weld tracking, an S-axis motor parallel to the Y-axis motor and a point LASER sensor connected to the S-axis motor are installed. Besides, the AVC axis motor is removed from the robot head. During the welding process, the S-axis motor drives the point LASER sensor to move reciprocally along the Y-direction to find the weld position. Figure 7 depicts the flow chart of the S-axis motor tracking weld. The LASER sensor returns the height value of its distance from the workpiece. After the S-axis motor moves forward, it determines whether there is a step change in the height of the workpiece by comparing the current LASER sensor return value with the LASER sensor return value of the previous step. If the step change of the workpiece height is regular, record the position of the S-axis motor as the position of the lap weld. The upper and lower limits displacement of S-axis motor operation is updated based on the position of the lap weld. Then, the S-axis motor runs in reverse. Until the S-axis motor exceeds the set lower limit of operation, the S-axis motor starts forward again. If the workpiece height has no step change and the S-axis motor exceeds the upper limit position, then the count is increased by 1. If the count is less than three times, the S-axis motor moves in reverse. If the count exceeds 3, the manual weld is identified and the welding is finished. During this time, the PLC receives the positions of the lap weld from the S-axis motor and then transmits the weld position information to the Y-axis. Then, the Y-axis motor moves along the weld positions and ultimately drives the movement of the welding gun in the Y direction.

As shown in Fig. 6, the robot path is usually defined by a series of discrete welding poses, $\{w_i | w_i = (P_i, R_i) \in SE(3), i \in \{1, \dots, N\}\}$, where $P_i \in R^3$ and $R_i \in SO(3)$ denote the tungsten electrode tip position and the welding gun orientation in the Cartesian coordinate system. Surface welding requires the robot to carry out precise contour motion, which requires the robot to move continuously and accurately along the contour defined in Cartesian space. In the robot controller, continuous linear segments of discrete reference commands are used to approximate the original curve contour. The generated surface welding path algorithm ensures that the welding gun position path and the welding gun direction path simultaneously execute discrete reference commands to achieve the smooth motion of the robot.

Fig. 7 Flowchart of S-axis motor weld tracking



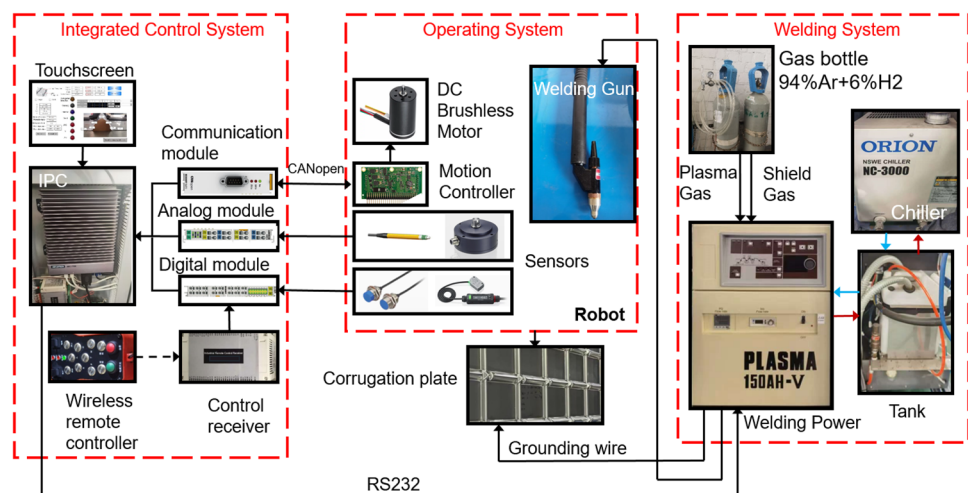
5 Experiment and application

5.1 Experiment of weld seam tracking

The whole system of welding seam recognition and tracking mainly includes the operating system, integrated control system, and welding system. The operator sets welding parameters on the touchscreen. The control system transmits current parameters to the welding power. The welding power supplies power to the welding gun and provides plasma gas and shield gas for welding. The sensors transmit the collected weld position information to the communication module of the control system. The control system transmits the error value between the sensor and the actual position of the welding gun to the motor driver in the operating system. The motor driver controls the rotation of the motor and ultimately the movement of the welding gun. The relationship diagram of each part of the welding robot system is shown in Fig. 8.

During the welding process, the sensor feeds back the real-time distance between the welding gun and the surface of the corrugated plate to the industrial computer. The industrial computer controls servo motors to complete precision welding. Figure 9 shows the comparison of the actual tracking displacement and angle curves with the theoretical displacement and angle curves when the robot welds large and small corrugated plates, and plots the error curve formed by the actual and theoretical differences. By reading the position information of the motor encoder, the actual tracked displacement curves of the Z-direction and X-direction can be obtained. By reading the value of the angle sensor, the actual angle curves can be obtained. Figure 9a presents a comparison of the actual and theoretical tracked displacement curves of the welding gun in the Z-direction. When the robot tracked the corrugated section, the displacement of the vertical direction turned bigger, then smaller. The peak points of the large and small corrugated displacement curves are 54 mm and 35 mm respectively. Figure 9b illustrates a comparison of the actual and theoretical displacement curves for welding large and small corrugated plates in the X-direction. Figure 9c compares the actual and theoretical angle curves for large and small corrugated plates in the R-rotation angle direction. The figures show that the displacement curves for each direction of movement were continuous and smooth during motion which reflects that the velocity changes were relatively uniform and the impact was relatively small, meaning that the mechanism had good stability during motion. In Fig. 9d–f, we compare the tracking dynamic precision of large and small corrugated plates. After lap weld seams are welded, calculate the error between the theoretical value and actual value in the Z-direction, X-direction, and R-rotation angle direction. The experiment results are shown in Fig. 9, where X-direction displacement has the highest dynamic precision for whatever large or small corrugated plate with automatic welding since its error fluctuation range $[-0.5, 0.5]$ is the smallest one. The experimental results show that the welding angle error within $\pm 5^\circ$ was smaller than the literature range [19]. The errors were within ± 1 mm or $\pm 5^\circ$, so the robot tracked lap weld with high accuracy and good reliability. The figures show that the actual welding results for the robot system had the same variation trend as the results from the theoretical displacement. The position and orientation approximation errors with the two size schemes remain within the related literature error tolerance limits, which verifies the error-controllable capability of the proposed control algorithm.

Fig. 8 The whole system of welding seam recognition and tracking



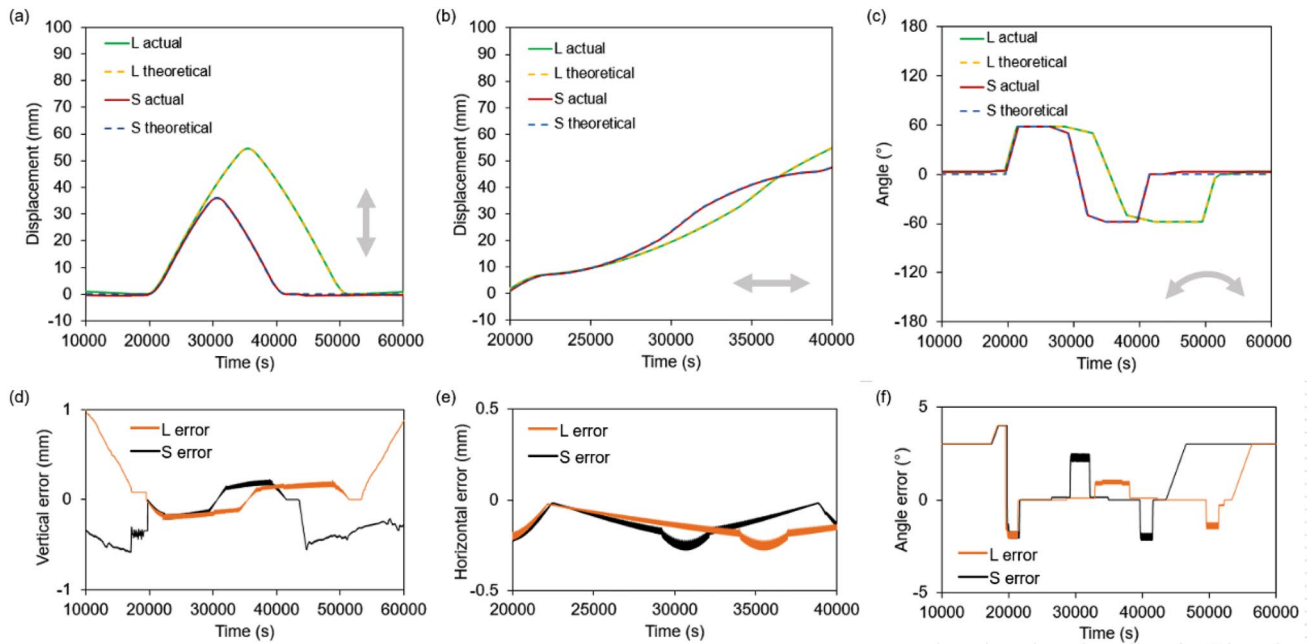


Fig. 9 Comparison of dynamic precision for large (L) and small (S) corrugations **a** the comparison of the actual and theoretical displacement in the Z-direction, **b** the comparison of the actual and theoretical displacement in the X-direction, **c** the comparison of the actual and theoretical angle curves, **d** the displacement curves of the vertical error for large and small corrugations, **e** the displacement curves of the horizontal error for large and small corrugations, **f** the angle deviation curves of the angle error for large and small corrugations

5.2 Experiment of quality stability

The welding qualification rate reflects the stability of welding quality. To calculate the welding qualified rate during ship production, the weld length is typically taken into account. The qualified rate is determined using the following formula:

$$P = \left(1 - \frac{L_d}{L_w}\right) \times 100\% = \left(1 - \frac{N_d \times l_m}{N_k \times l_k}\right) \times 100\% \quad (2)$$

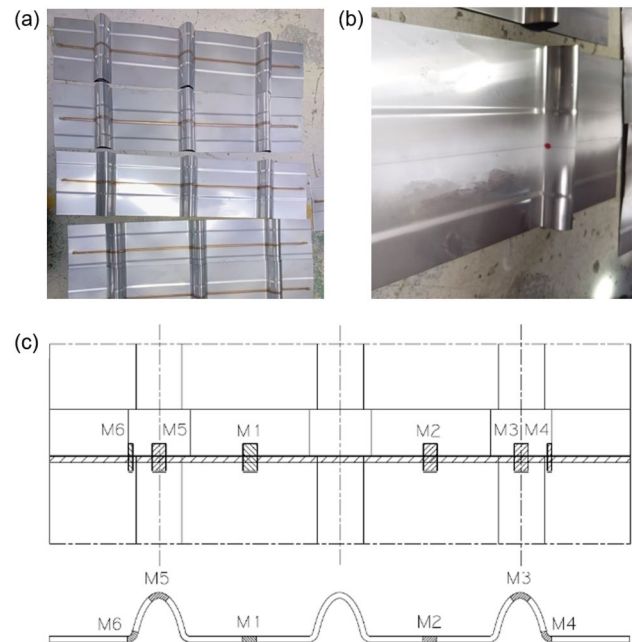
where P is the welding qualified rate. L_d is the length of weld defect, L_w is the total length of welds, N_d is the number of welding defect locations, N_k is the cumulative number of welded corrugated plates, l_k is the total weld length of each plate, and l_m is the repair length of each defect.

For this experiment, the total length and width of each test plate were 100 cm and 25 cm (Fig. 10a). The repair length of a defect was approximately 2 cm. The red dots appear at the defect by using the developer (Fig. 10b). A total of 254 corrugated plates were welded, resulting in 29 welding defects. Of these defects, 16 were attributed to gaps in the assembly, which were unrelated to the performance of the welding robot. Based on these parameters, the welding qualified rate was calculated to be 99%.

5.3 Welding procedure qualification test and endurance test

To enter the LNG carrier construction market, it is necessary to obtain the welding qualification certification of the French company Gaztransport & Technigaz (GTT). According to the GTT file, the welding procedure qualification test was carried out. The weld seam's appearance was first checked, and it was observed that the width of the weld pass falls between 3 mm and 6.5 mm. The front weld is full, and there are no visible defects such as porosity or non-fusion. The back also did not exhibit any burn-through. After the appearance check, Penetrant Testing (PT) was performed on the welds following the GTT file's procedures. The PT inspection of the weld seam involves three main steps: (i) Applying penetrant on the surface of the weld seam. The penetrant will penetrate the surface opening defects via capillary action after a short period. (ii) Cleaning the excess penetrant on the surface of the weld seam using detergent. (iii) Applying the developer,

Fig. 10 Experiment of quality stability and weld section position diagram **a** Test plates, **b** Red dots appearance in the developer, **c** Weld section position diagram of GTT metallographic inspection



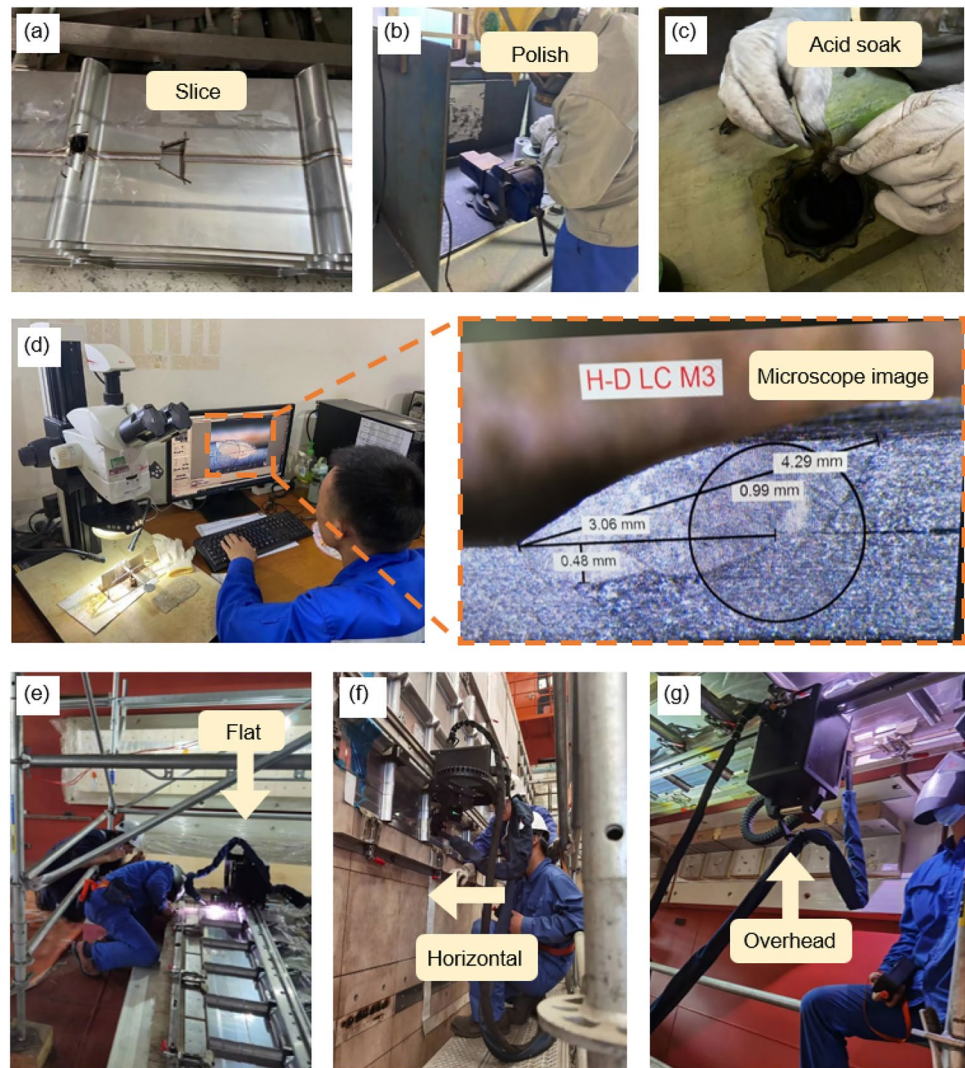
which attracts the penetrant in the defects and reveals the defects. The penetrant will be trapped in the defects to show the pink morphology by the developer (Fig. 10b). After the PT is performed, the test plates are sliced at six designated locations according to the GTT metallographic test documentation (Fig. 10c). The metallographic inspection process goes through four main steps. Firstly, the trapezoidal shape slices are selected from six positions, as depicted in Fig. 11a. Secondly, the cross-section is ground and polished as shown in Fig. 11b. Thirdly, an acid soak is applied to improve the clarity of the resulting image, as illustrated in Fig. 11c. Finally, the width, throat, and depth of the weld seam are determined by examining microscope images, as demonstrated in Fig. 11d. Based on the analysis of metallographic inspection results, the resulting weld pool width exceeded 2 mm, the weld throat was greater than 0.7 mm, the penetration depth ranged between 0.4 mm and 1.2 mm, and the weld surface width was between 3.5 mm and 6 mm. These results confirm that the metallographic results are in accordance with the requirements.

Based on the GTT document specifications, the simulated cabin's durability test requires welding four large plates of 1 m × 3 m. These plates are used to conduct flat (Fig. 11e), horizontal (Fig. 11f), vertical, and overhead welding tests (Fig. 11g). It takes an average of 3 min and 40 s to weld a 1 m seam, and each position takes approximately 40 min to weld. Once the welding appearance is checked, six locations on each weld seam are selected for cutting and metallographic testing, as required by the document. A total of 16 welds at four positions were tested, and the metallographic results obtained from 96 small plates numbered M1 to M6 met the requirements of GTT, which means the endurance test has been passed.

6 Conclusions

A novel five-axis welding robot based on a surface tracking control system is designed for welding various curvature types of corrugated structures, which can realize flat, horizontal, vertical, and overhead automatic welding in LNG cargo containment. A new tracking sensor system based on a LASER sensor, two contact sensors, and an angle sensor is designed to realize multiple functions, including tracking the welding arc length, identifying corrugation shapes, and detecting welding gun posture. The sensing system can cooperate with the robot control system to complete welding seam tracking, adjustment and control of welding gun spatial posture. Based on the devised tracking sensor system and welding robot, a robot servo-control system with a surface tracking welding control algorithm is constructed. The experimental results of weld seam tracking reflect the control effect of the robot servo-control system on the position and posture of the welding gun. The control errors of the welding gun were within ± 1 mm or $\pm 5^\circ$. The welding qualification rate reaches 99% and the standard workload of automatic welding is about 7 times that of

Fig. 11 GTT metallographic inspection and welding test **a** weld section position diagram, **b** cross-section grinding diagram, **c** acid soaking, **d** microscopic observation, **e** flat position welding, **f** horizontal position welding, **g** Overhead position welding



manual welding, which reflects that the five-axis robotic tracking system can complete the welding of corrugated structures in the cargo containment with high quality and high efficiency welding.

Acknowledgements This work is supported by the Ministry of Industry and Information Technology of the People's Republic of China ([2020] No. 313).

Author contributions YC: Conceptualization, Methodology, Supervision, Writing – original draft, Writing – review & editing. KM: Conceptualization, Formal analysis, Data Curation, Writing – original draft, Writing – review & editing. LZ: Methodology, Data Curation, Resources, Investigation, Funding acquisition. JX: Methodology, Software, Resources, Investigation, Funding acquisition. WZ: Resources, Investigation, Project administration, Supervision. XW: Software, Project administration, Supervision. HG: Investigation, Software, Supervision. YZ: Project administration, Funding acquisition, Supervision.

Funding This research has been supported by the High-Tech Ship Scientific Research Project of MIIT ([2020] No.313).

Data availability The main data supporting the results of this study are available within the paper. Raw preprocessed data for Fig. 9 is provided at <https://doi.org/10.6084/m9.figshare.24448522>.

Declarations

Competing interests The authors declare no competing interests.

Open Access This article is licensed under a Creative Commons Attribution 4.0 International License, which permits use, sharing, adaptation, distribution and reproduction in any medium or format, as long as you give appropriate credit to the original author(s) and the source, provide a link to the Creative Commons licence, and indicate if changes were made. The images or other third party material in this article are included in the article's Creative Commons licence, unless indicated otherwise in a credit line to the material. If material is not included in the article's Creative Commons licence and your intended use is not permitted by statutory regulation or exceeds the permitted use, you will need to obtain permission directly from the copyright holder. To view a copy of this licence, visit <http://creativecommons.org/licenses/by/4.0/>.

References

1. Kumar S, Kwon H-T, Choi K-H, et al. LNG: an eco-friendly cryogenic fuel for sustainable development. *Appl Energy*. 2011;88(12):4264–73. <https://doi.org/10.1016/j.apenergy.2011.06.035>.
2. Zalar M, Diebold L, Selected Hydrodynamic Issues in Design of Large LNG Carriers, in: RINA ICSOT, Busan, South Korea., 2006.
3. He T, Chong ZR, Zheng J, et al. LNG cold energy utilization: prospects and challenges. *Energy*. 2019;170:557–68. <https://doi.org/10.1016/j.energy.2018.12.170>.
4. Graczyk M, Moan T, Wu M. Extreme sloshing and whipping-induced pressures and structural response in membrane LNG tanks. *Ships Offshore Struct*. 2007;2(3):201–16. <https://doi.org/10.1080/17445300701423049>.
5. Choe J, Kim KH, Lee D, et al. Glass composite vibration isolating structure for the LNG cargo containment system. *Compos Struct*. 2014;107:469–75. <https://doi.org/10.1016/j.compstruct.2013.08.013>.
6. Yu YH, Kim BG, Lee DG. Cryogenic reliability of composite insulation panels for liquefied natural gas (LNG) ships. *Compos Struct*. 2012;94(2):462–8. <https://doi.org/10.1016/j.compstruct.2011.08.009>.
7. Lee D-H, Ha M-K, Kim S-Y, et al. Research of design challenges and new technologies for floating LNG. *Int J Naval Archit Ocean Eng*. 2014;6(2):307–22. <https://doi.org/10.2478/IJNAOE-2013-0181>.
8. Kim M-S, Kwon S-B, Kim S-K, et al. Impact failure analysis of corrugated steel plate in LNG containment cargo system. *J Constr Steel Res*. 2019;156:287–301. <https://doi.org/10.1016/j.jcsr.2019.02.008>.
9. Lee D, Yoon SH, Kim KH, et al. Composite anti-buckling structure for the corrugations of liquefied hydrogen containers. *Compos Struct*. 2013;95:492–9. <https://doi.org/10.1016/j.compstruct.2012.07.004>.
10. Ang MH Jr, Lin W, Lim S. Walk-through programmed robot for welding in shipyards. *Ind Robot Int J*. 1999;26:377–88. <https://doi.org/10.1108/01439919910284000>.
11. Lee D, Lee S, Ku N, et al. Development of a mobile robotic system for working in the double-hulled structure of a ship. *Robot Comput Integr Manuf*. 2010;26(1):13–23. <https://doi.org/10.1016/j.rcim.2009.01.003>.
12. Ku N, Cha J-h, Lee K-Y, et al. Development of a mobile welding robot for double-hull structures in shipbuilding. *J Mar Sci Technol*. 2010;15(4):374–85. <https://doi.org/10.1007/s00773-010-0099-5>.
13. Rout A, Deepak BBVL, Biswal BB. Advances in weld seam tracking techniques for robotic welding: a review. *Robot Comput Integr Manuf*. 2019;56:12–37. <https://doi.org/10.1016/j.rcim.2018.08.003>.
14. Li X, Li X, Khyam MO, et al. Robust welding seam tracking and recognition. *IEEE Sens J*. 2017;17(17):5609–17. <https://doi.org/10.1109/JSEN.2017.2730280>.
15. Chen S, Liu J, Chen B, et al. Universal fillet weld joint recognition and positioning for robot welding using structured light. *Robot Comput Integr Manuf*. 2022;74:102279. <https://doi.org/10.1016/j.rcim.2021.102279>.
16. Lei T, Rong Y, Wang H, et al. A review of vision-aided robotic welding. *Comput Ind*. 2020;123:103326. <https://doi.org/10.1016/j.compind.2020.103326>.
17. Hong TS, Ghobakhloo M, Khaksar W. 6.04–Robotic welding technology. *Compr Mater Process*. 2014. <https://doi.org/10.1016/B978-0-08-096532-1.00604-X>.
18. Lee D Y, Jung J H, Han S H, et al. (2004) Spider robot - automatic transfer system of the plasma welding machine for LNGC membrane sheet. *SICE 2004 Annual Conference 2:1880–1884 vol. 1882*.
19. Yi J, Qingqing H, Zhaoen D, et al. Structural design and kinematic analysis of a welding robot for liquefied natural gas membrane tank automatic welding. *Int J Adv Manuf Technol*. 2022;122:1–14. <https://doi.org/10.1007/s00170-022-09861-2>.
20. Guo L, Zhang H. Autonomous mobile welding robot for discontinuous weld seam recognition and tracking. *Int J Adv Manuf Technol*. 2022. <https://doi.org/10.1007/s00170-021-08616-9>.
21. Lee D, Ku N, Kim TW, et al. Development and application of an intelligent welding robot system for shipbuilding. *Robot Comput Integr Manuf*. 2011;27(2):377–88. <https://doi.org/10.1016/j.rcim.2010.08.006>.
22. Guo J, Zhu Z, Sun B, et al. A novel field box girder welding robot and realization of all-position welding process based on visual servoing. *J Manuf Process*. 2021;63:70–9. <https://doi.org/10.1016/j.jmapro.2020.04.054>.
23. Le J, Zhang H, Chen X. Realization of rectangular fillet weld tracking based on rotating arc sensors and analysis of experimental results in gas metal arc welding. *Robot Comput Integr Manuf*. 2018;49:263–76. <https://doi.org/10.1016/j.rcim.2017.06.004>.
24. Xu F, Xu Y, Zhang H, et al. Application of sensing technology in intelligent robotic arc welding: a review. *J Manuf Process*. 2022;79:854–80. <https://doi.org/10.1016/j.jmapro.2022.05.029>.

Publisher's Note Springer Nature remains neutral with regard to jurisdictional claims in published maps and institutional affiliations.